Available online at www.sciencedirect.com
ScienceDirect
Acta Biomaterialia 5 (2009) 607–612
Acta BIOMATERIALIA
www.elsevier.com/locate/actabiomat

Brief communication

Capture of bacteria by flexible carbon nanotubes

Tsukasa Akasaka *, Fumio Watari

Department of Biomedical, Dental Materials and Engineering, Graduate School of Dental Medicine, Hokkaido University, Kita 13 Nishi 7, Kita-ku, Sapporo 060-8586, Japan

Received 17 April 2008; received in revised form 18 July 2008; accepted 19 August 2008
Available online 9 September 2008

Abstract

Capture of bacteria with flexible carbon nanotubes (CNTs) was done in vitro. Bundles of single-walled carbon nanotubes (SWCNTs) or multi-walled carbon nanotubes (MWCNTs) was mixed with *Streptococcus mutans*. Precipitation assays and colony-forming unit formation assays showed free *S. mutans* in the solution was significantly decreased by the addition of the CNTs. Observation of the precipitate by scanning electron microscopy showed bacterial adhesion to CNTs. It has been shown that CNTs of different diameters have significantly different effects on the precipitation efficiency, and the manners in which they capture the cells are different. We found that MWCNTs (diameter of approximately 30 nm) had the highest precipitation efficiency, which was attributable to both their adequate dispersibility and aggregation activity. From observations by scanning electron microscopy, bundles of SWCNTs and thin MWCNTs (diameter of approximately 30 nm), which were moderately flexible, were easily wound around the curved surface of *S. mutans*. Bare CNTs having high adhesive ability could be useful as biomaterials, e.g., as tools for the elimination of oral pathogens at the nano-level.

Keywords: Carbon nanotubes; Bacteria; *Streptococcus mutans*; Adhesion

1. Introduction

Many carbon materials exhibit excellent molecular adsorption properties, and activated carbon (AC) [1], which is widely used as an adsorbent, has a high capacity for adsorption owing to its porous structure and large surface area. The occurrence of dental caries is mainly associated with oral pathogens, and *Streptococcus mutans* is a primary cariogenic organism. Therefore, many attempts have been made to eliminate *S. mutans* from the oral cavity. One effective way is to use AC as an adsorbent, hence it is used in a wide range of oral care products, such as toothpastes and mouthwashes [2,3].

Carbon nanotubes (CNTs) have attracted considerable attention because of their unique physical properties and potential for a variety of biological applications [4]. In recent investigations, CNTs have been utilized as adsorbents to eliminate dyes [5]. In addition, CNTs can adsorb bacteria [6–8]; single-walled carbon nanotubes (SWCNTs) exhibit strong antimicrobial activity toward *Escherichia coli* [9,10]. However, bacterial adhesion, particularly oral bacterial adhesion, to CNTs has not yet been sufficiently investigated. If bare CNTs are found to have strong adhesive activity and winding CNTs bind oral pathogens, they may be useful as tools at the nano-level for capturing oral pathogens. In this study, we investigated oral bacterial adhesion to CNTs of different diameters and flexibility, and compared them with the widely used adsorbent AC particles. In general, SWCNTs with diameter of approximately 1 nm are known to be highly flexible, while multi-walled carbon nanotubes (MWCNTs) with diameters >100 nm are hard. Here we report that CNTs with different diameters have significantly different effects on the efficiency of *S. mutans* precipitation, that the manners in which they capture bacteria are different and that bundles of SWCNTs and MWCNTs with average diameters of 30 nm can wind around the curved surfaces of bacteria.

* Corresponding author. Tel./fax: +81 11 706 4251.
E-mail address: akasaka@den.hokudai.ac.jp (T. Akasaka).

1742-7061/$ - see front matter © 2008 Acta Materialia Inc. Published by Elsevier Ltd. All rights reserved.
doi:10.1016/j.actbio.2008.08.014

2. Experimental

The SWCNTs employed were synthesized by an arc discharge method. The MWCNTs used were of two types: 30-MWCNTs (average diameter of 30 nm; produced by NanoLab Inc., Brighton, MA) and 200-MWCNTs (average diameter of 200 nm; produced by MTR Co. Ltd., OH). As a control carbon sample, a commercial activated carbon powder (AC) with an average particle size of 20 μm (Kanto Chemical Co. Inc., Tokyo, Japan) was used in this study. *S. mutans* JC2 was grown aerobically in brain heart infusion (BHI) broth at 37 °C for several days. The bacteria were harvested by centrifugation at 2500*g* (Kubota Centrifuge 2700), washed in phosphate-buffered saline (PBS: 20 mM K_2HPO_4/KH_2PO_4, 150 mM NaCl, pH 7.4) and suspended in the same buffer to an optical density (OD) of 1.0 at 700 nm.

For a bacterial precipitation assay, 6 ml of a suspension of CNTs treated by ultrasonication in PBS was added to 3 ml of the bacterial suspension in a glass bottle. As a control, PBS solution was used in substitution for CNTs solutions (initial OD of final volume was 0.34; 1.4×10^8 colony-forming units (CFU) ml^{-1}). The solution was shaken at 200 rpm for 20 min by a universal shaker (Iwaki SHK-U3) and then centrifuged at 100*g* for 3 min. A 2 ml sample of the upper suspension was transferred to a quartz cell, and the OD at 700 nm was measured with an ultraviolet–visible spectrometer.

To identify the suspended carbon of the supernatant after centrifugation, aliquots of the supernatant at a carbon sample concentration of 0.66 mg ml^{-1} were dried on a slide glass. The dry substances were sputtered using a carbon coater (Meiwa Shoji CC-40F) and then examined by scanning electron microscopy (SEM; Hitachi S4000). For a CFU formation assay of the supernatant after centrifugation, a 1 ml sample of each supernatant carbon sample at concentration of 0.66 mg ml^{-1} was used. Upon serial dilution, the diluted samples (10 μl each in triplicate) were spread evenly onto solid BHI medium plates for aerobic incubation at 37 °C for 3 days, and the colonies were then counted.

For SEM observation of the precipitate after centrifugation, the precipitate was collected on a polycarbonate filter (Advantec, 0.8 μm in pore size) and immersed in a fixative (2% glutaraldehyde in PBS) for 2 h. The samples were dehydrated in graded ethanol and dried with CO_2 in a critical point dryer (Hitachi HCP-1). The cells were sputtered using a carbon coater and then examined by SEM.

3. Results and discussion

The adhesive activities of the CNTs were assessed by a bacterial precipitation assay using *S. mutans*. The results of the precipitation assay are presented in Fig. 1a and b. When the bacterial suspensions were mixed with the CNTs, there was loss in supernatant turbidity with an increase in the amount of CNTs. The results clearly show that CNTs have adhesive ability. These results regarding *S. mutans* adhesion to CNTs are in agreement with the previously reported results regarding bacterial adhesion to CNTs in the case of *E. coli* [7–10]. Among the carbon samples, the precipitation efficiency of 30-MWCNTs was the highest, with a maximum at 0.17 mg ml^{-1} concentration. SWCNTs were less effective because they were not easily dispersed

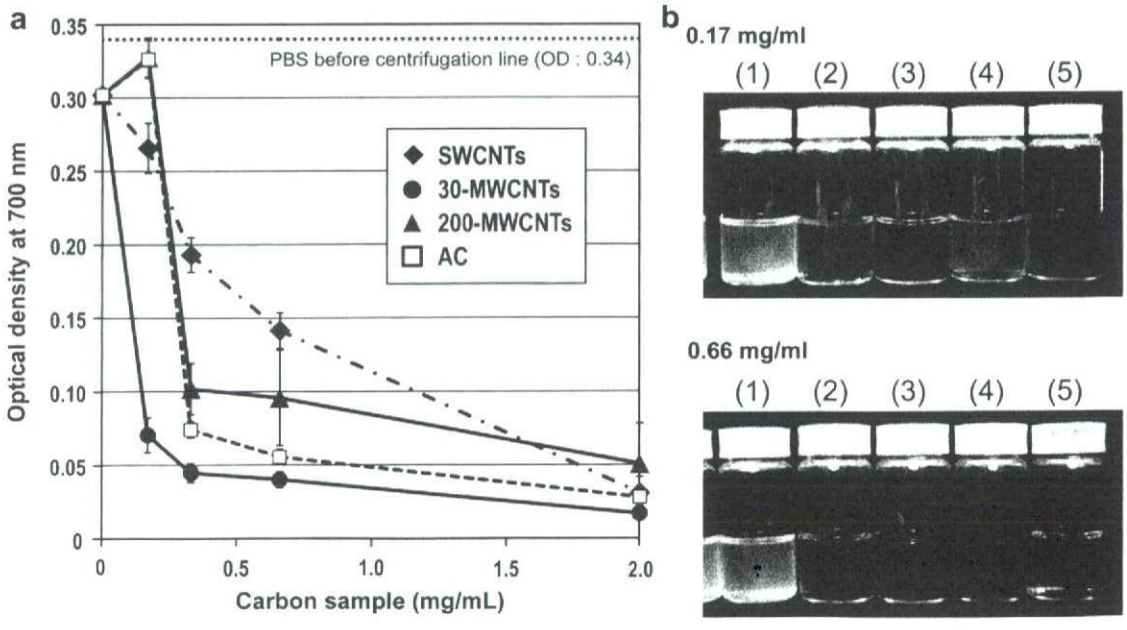

Fig. 1. (a) OD (at 700 nm) of the supernatant in precipitation assay with carbon samples. Results are presented as means ± SE of three experiments. The upper dotted line is the OD value (0.34) of PBS before centrifugation (control). (b) Photographs of *S. mutans* mixed with carbon samples: PBS (b-1); SWCNTs (b-2); 30-MWCNTs (b-3); 200-MWCNTs (b-4); AC (b-5) after centrifugation.

before mixing with the bacteria; and 200-MWCNTs seemed to be less effective because some of them did not precipitate but remained suspended in the solution.

Fig. 2 shows that the number of free *S. mutans* and/or *S. mutans* adhering to suspended carbon samples depends on the type of carbon sample employed. A considerable number of free bacteria were observed with PBS and SWCNTs. However, few free bacteria were observed with 30-MWCNTs, 200-MWCNTs and AC. Moreover, with 200-MWCNTs and AC, a comparatively large amount of suspended carbon was observed. In the AC, small particles (particle size 1–10 μm) were observed in the AC particles. These carbon suspensions occur when bacteria or bacterial products act as surfactants. It was found that 200-MWCNTs were strongly adhesive to bacteria but showed poor precipitation in the bacterial suspension.

To remove the influence of the suspended carbon samples in the supernatant on the assessment of bacterial adhesion, the residual amount of bacteria was evaluated by CFU formation assay. The percentage of CFUs referenced to the control is shown in Fig. 3. The number of free bacteria decreased for all carbon samples, reaching reductions of 65–96% from the initial numbers of bacteria in the suspension. In particular, 30-MWCNTs and 200-MWCNTs bring about the highest decrements, of 92% and 96%, respectively. This result shows that 30-MWCNTs and 200-MWCNTs are highly adhesive to bacteria. However, 200-MWCNTs did not readily precipitate from suspension, a large amount of them remaining suspended in the supernatant (Fig. 2d), with the OD value of the supernatant being comparatively high (Fig. 1).

Kim et al. [7] reported that CNT clusters show high affinity toward and bind *E. coli* cells. No significant

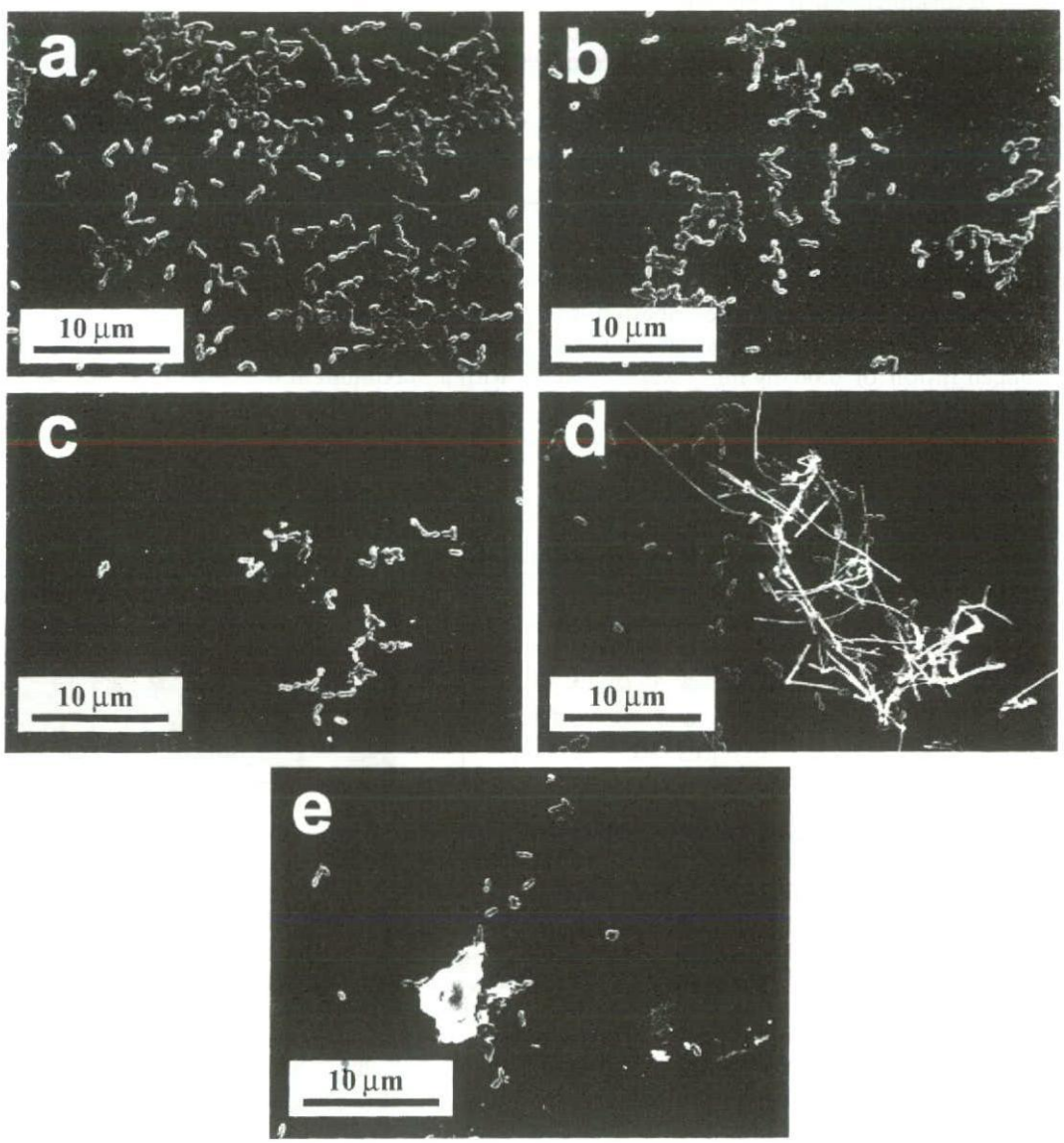

Fig. 2. SEM images of dried supernatant on a slide glass after mixing with carbon samples at a concentration of 0.66 mg ml^{-1}: PBS (a); SWCNTs (b); 30-MWCNTs (c); 200-MWCNTs (d); AC (e).

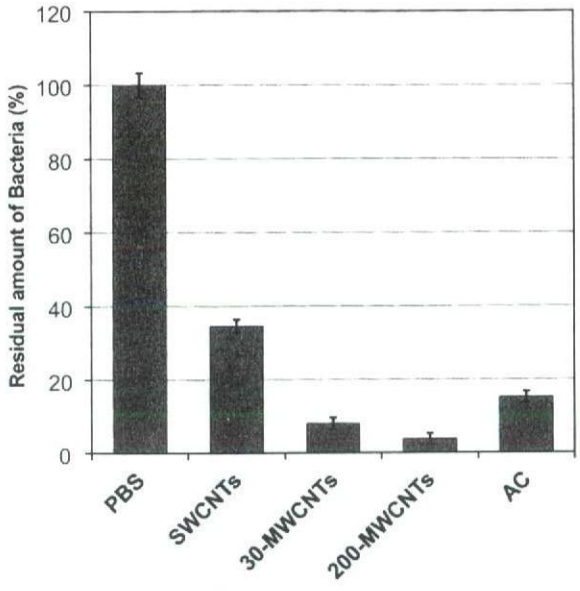

Fig. 3. Residual amount of *S. mutans* in the supernatant after mixing with carbon samples at 0.66 mg ml^{-1} concentration. Results are presented as means ± SE of three experiments.

difference in the affinity of bacterial adhesion was observed between SWCNTs and MWCNTs. The results of the precipitation assay may be influenced by the aggregation activity of each carbon material, which in turn depends on the differences in their diameters. Bacteria are known to attach to AC particles by means of strong van der Waals forces between the bacterial and the carbon surfaces [11]. Therefore, all types of carbon material will have a high affinity to bacteria because of the generation of van der Waals forces. However, carbon materials with strong aggregation activity, such as SWCNTs, are not readily dispersed in hydrophilic solution and thus, decrease the area available for bacterial adhesion. In contrast, carbon materials with weak aggregation activity, such as 200-MWCNTs and AC, in the limited size range used in this study are not readily precipitated from hydrophilic solution. Our results show 30-MWCNTs had the highest precipitation efficiency, which was attributable to both their adequate dispersibility and aggregation activity.

Subsequently, bacterial adhesion to the CNTs of different diameters in the precipitates was observed by SEM. Fig. 4 shows SEM image of *S. mutans* adhered to CNTs or AC in the precipitates. Several *S. mutans* cells adhered to the meshwork comprising rope-like bundles of SWCNTs, with an average diameter of about 100 nm. Similar to the fibrous shape of the bundles of SWCNTs, fibrous extracellular polymeric substances (width of about 10 nm) were also observed at right-angles to the bacterial surface (the black arrows in Fig. 4). Furthermore, it is notable that some of the bundles wound around the curved surfaces of the *S. mutans* cells (Fig. 4a and b). Thus, the flexibility of the bundles seems to be greater than that of the bacterial cell wall. Sano et al. [12] reported that SWCNTs are worm-like polymers in solution and have flexibility. Therefore, SWCNTs can adjust their structure to follow the surface morphology of *S. mutans* (radius of minor axis: 500 nm). Fig. 4a clearly shows that a bundle of SWCNTs captured *S. mutans* passing through a pore of a membrane filter. A flexible net of SWCNTs can be strongly bent without breaking. In a similar manner, 30-MWCNTs (average diameter of 30 nm) captured *S. mutans* and wound around the curved surface of *S. mutans* (Fig. 4c). Poncharal et al. [13] reported that the ripple structure in the tube caused the MWCNTs (diameter of ~30 nm) to bend uniformly, with a radius of curvature of 400 nm. 30-MWCNTs could wind around the bacteria with the ripple structure. In contrast, though the 200-MWCNTs (average diameter of 200 nm) also adhered to the cells, they did not wind around the surface of *S. mutans* (Fig. 4d). Thus, the flexibility of 200-MWCNTs seems to be less than that of the bacterial cell wall. As for the control material (Fig. 4e), bacterial adhesion occurred at the surface of AC (average particle size 20 μm).

Further, rounded bacteria adhered to SWCNTs under these conditions. This observation contradicts the previous result that flattened cells are inactivated on SWCNTs, which was reported by Kang et al. [9,10] and Brady-Estévez et al. [14]. The differences in morphology could depend on the differences between Gram-positive bacteria, which have a thick cell wall (such as *S. mutans*), and Gram-negative bacteria, which have a thin cell wall (such as *E. coli*), or on the purity of SWCNTs. In addition, CNTs winding around bacteria have not been clearly observed in previous studies [7,9]. This could be explained by the difference between Gram-positive and Gram-negative bacteria or by the use of different procedures for mixing bacteria with CNTs.

In our study, data from both the precipitation assay and SEM images prove that CNTs can adhere to *S. mutans*. Although all types of carbon materials show high affinity toward bacteria because of the generation of van der Waals forces, it has been shown that CNTs of different diameters have significantly different effects on the precipitation efficiency, and the ways in which they capture cells are different. We found that 30-MWCNTs had the highest precipitation efficiency, which was attributable to both their adequate dispersibility and aggregation activity. This may be attributed to differences in the flexibility of the nanotubes. The advantages of capturing pathogens by winding CNTs may be to ensure stronger adhesion and to inhibit the release and budding of captured bacteria. We believe that this could be one of the features of CNTs.

Although the optimum conditions for precipitation are still not clear, we have demonstrated that *S. mutans* can be captured by flexible CNTs. For capturing or eliminating bacteria, the use of CNTs that can adhere to bacteria via physical sorption is not linked to antimicrobial resistance. Bare CNTs having high adhesive ability could be useful as biomaterials, e.g., as tools for the elimination of oral pathogens at the nano-level.

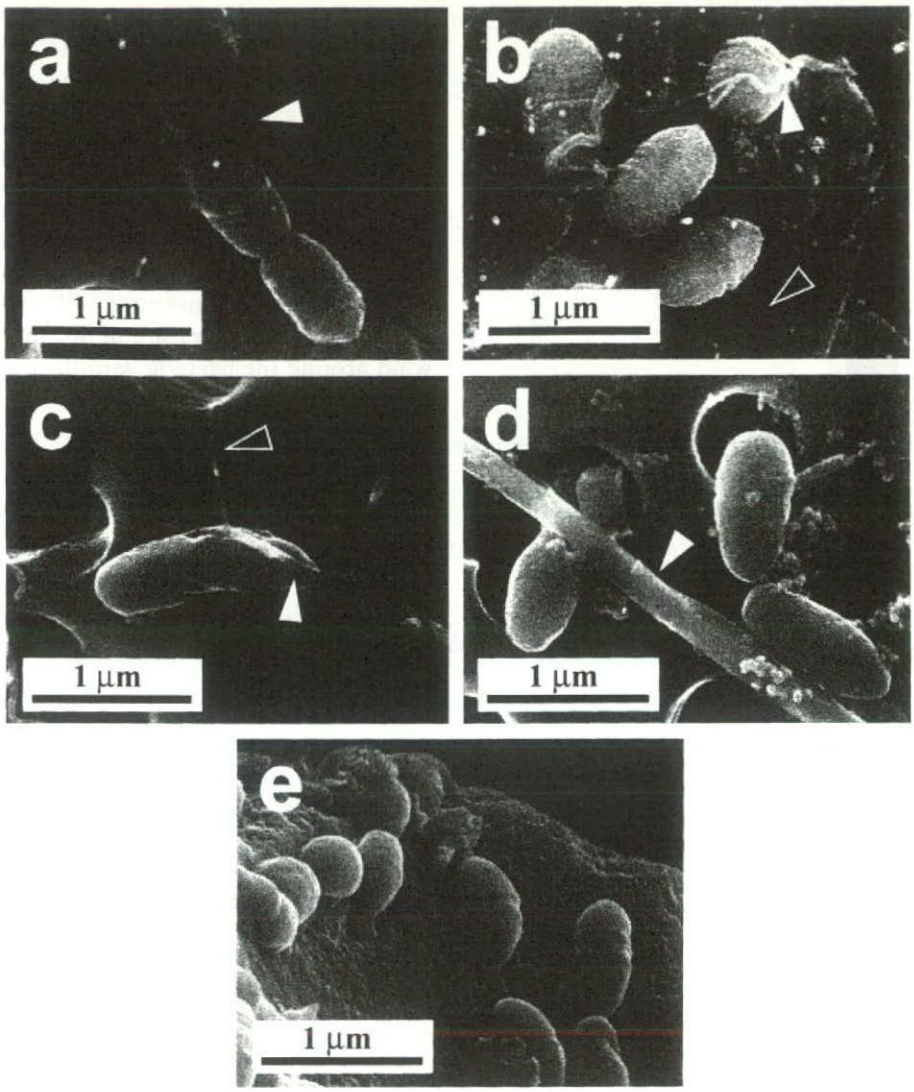

Fig. 4. SEM images of *S. mutans* adhered to CNTs or AC: bundles of SWCNTs wound around *S. mutans* (a); the bacteria adhered to the meshwork comprising bundles of SWCNTs (b); 30-MWCNTs wound around bacteria (c); 200-MWCNTs adhered but did not wind (d); AC surface adhered to bacteria (e). The white arrows indicate CNTs. The black arrows indicate fibrous substances produced by bacteria.

Acknowledgements

We thank Prof. Kazuyuki Tohji and Dr. Yoshinori Sato (Tohoku University) for providing the SWCNTs and Prof. Kenichirou Shibata (Hokkaido University) for donating the *S. mutans* JC2 strain used in this work. This study was supported by Health and Labour Science Research grants in 2006 (H18-kagaku-006) from the Ministry of Health, Labour and Welfare of Japan. Part of this work was also supported by a Grant-in-Aid for Scientific Research (No. 16791177) from the Ministry of Education, Culture, Sports, Science, and Technology of Japan.

References

[1] Pape HL, Solano-Serena F, Contini P, Devillers C, Maftah A, Leprat P. Evaluation of the anti-microbial properties of an activated carbon fibre supporting silver using a dynamic method. Carbon 2002;40:2947–54.

[2] Sarita PT, Tuominen R. Tooth cleaning methods and their effectiveness among adults in rural Tanzania. Proc Finn Dent Soc 1992;88:139–45.

[3] Camper AK, LeChevallier MW, Broadaway SC, McFeters A. Bacteria associated with granular activated carbon particles in drinking water. Appl Environ Microbiol 1986;52:434–8.

[4] Akasaka T, Watari F, Sato Y, Tohji K. Apatite formation on carbon nanotubes. Mater Sci Eng C 2006;26:675–8.

[5] Fugetsu B, Satoh S, Iles A, Tanaka K, Nishi N, Watari F. Encapsulation of multi-walled carbon nanotubes (MWCNTs) in Ba^{2+} -alginate to form coated micro-beads and their application to the pre-concentration/elimination of dibenzo-*p*-dioxin, dibenzofuran, and biphenyl from contaminated water. Analyst 2004;129:565–6.

[6] Srivastava A, Srivastava ON, Talapatra S, Vajtai R, Ajayan PM. Carbon nanotube filters. Nat Mater 2004;3:610–4.

[7] Kim JW, Shashkov EV, Galanzha EI, Kotagiri N, Zharov VP. Photothermal antimicrobial nanotherapy and nanodiagnostics with self-assembling carbon nanotube clusters. Lasers Surg Med 2007;39:622–34.

[8] Zharov VP, Galanzha EI, Shashkov EV, Kim J-W, Khlebtsov NG, Tuchin VV. Photoacoustic flow cytometry: principle and application for real-time detection of circulating single nanoparticles, pathogens, and contrast dyes in vivo. J Biomed Opt 2007;12:051503.

[9] Kang S, Pinault M, Pfefferle LD, Elimelech M. Single-walled carbon nanotubes exhibit strong antimicrobial activity. Langmuir 2007;23:8670–3.

[10] Kang S, Herzberg M, Rodrigues DF, Elimelech M. Antibacterial effects of carbon nanotubes: size does matter! Langmuir 2008;24:6409–13.

[11] Busscher HJ, Dijkstra RJB, Langworthy DE, Collias DI, Bjorkquist DW, Mitchell MD, et al. Interaction forces between waterborne bacteria and activated carbon particles. J Colloid Interface Sci 2008;322:351–7.

[12] Sano M, Kamino A, Okamura J, Shinkai S. Noncovalent self-assembly of carbon nanotubes for construction of "cages". Nano Lett 2002;2:531–3.

[13] Poncharal P, Wang ZL, Ugarte D, de Heer WA. Electrostatic deflections and electromechanical resonances of carbon nanotubes. Science 1999;283:1513–6.

[14] Brady-Estévez AS, Kang S, Elimelech M. A single-walled-carbon-nanotube filter for removal of viral and bacterial pathogens. Small 2008;4:481–4.

Available online at www.sciencedirect.com
ScienceDirect
Acta Biomaterialia 3 (2007) 669–675
Acta BIOMATERIALIA
www.elsevier.com/locate/actabiomat

Self-assembly of nano-hydroxyapatite on multi-walled carbon nanotubes

Susan Liao [a,b,*], Guofu Xu [c], Wei Wang [d], Fumio Watari [d], Fuzhai Cui [e], Seeram Ramakrishna [a,f], Casey K. Chan [a,b]

[a] *Nanoscience and Nanotechnology Initiative, Division of Bioengineering, Faculty of Engineering, National University of Singapore, Singapore 117576, Singapore*
[b] *Department of Orthopaedic Surgery, Yong Loo Lin School of Medicine, National University of Singapore, Singapore 119074, Singapore*
[c] *School of Materials Science and Engineering, Central South University, Changsha 410083, China*
[d] *Graduate School of Dental Medicine, Hokkaido University, Sapporo 060-8586, Japan*
[e] *Department of Materials Science and Engineering, Tsinghua University, Beijing 100084, China*
[f] *Department of Mechanical Engineering, Faculty of Engineering, National University of Singapore, Singapore 117576, Singapore*

Received 3 October 2006; received in revised form 9 March 2007; accepted 16 March 2007
Available online 18 May 2007

Abstract

Inspired by self-assembly of nano-hydroxyapatite (nHA) on collagen associated with the 67 nm periodic microstructure of collagen, we used multi-walled carbon nanotubes (MWCNTs) with approximately 40 nm bamboo periodic microstructure as a template for nHA deposition to form a nHA–MWCNT composite. The assembled apatite was analyzed by transmission electron microscopy and scanning electron microscopy. Defects that were analogous to edge dislocations along the carbon nanotubes' multi-walled surfaces were the nucleation sites for nHA after these defects had been functionalized principally into carboxylic groups. Spindle-shaped units consisting of an assembly of near parallel, fibril-like nHA polycrystals were formed and oriented at a certain angle to the long axis of the carbon nanotubes, unlike nHA–collagen in which the nHA is oriented along the longitudinal axis of the collagen molecule. One possible explanation for this difference is that there are more bonds for calcium chelation (–COOH, >C=O) on the collagen fibril surface than on the surface of MWCNTs. Spindle-shaped units that are detached from the MWCNT template are able to maintain the ordered parallel structure of the nHA polycrystal fibril. We have thus created a self-assembled hydroxyapatite on MWCNTs.

Keywords: Carbon nanotubes; Nano-hydroxyapatite; Bioinspired; Self-assembly; Collagen

1. Introduction

Various models have been designed to simulate the collagen mineralization process from the gene to the peptide level using a range of materials from natural extracellular matrix to synthetic polymers. Such investigations aim to study the basic mechanisms of biomineralization. Moreover, insights and understanding of these mechanisms will enable better design and fabrication strategies for nanocomposites to be used for hard tissue (bone and teeth) repair and replacement [1–8]. Zhang focused on fabricating self-assembling peptides and protein nanofibers. He showed that surfactant-like peptides (~2 nm in size) could self-assemble into nanotubes with a diameter of ~30–50 nm, which then formed an interconnected network similar to that observed in carbon nanotubes [3]. Stupp and colleagues developed a peptide–amphiphile model to study the self-assembly and mineralization mechanisms.

* Corresponding author. Address: Nanoscience and Nanotechnology Initiative, Division of Bioengineering, Faculty of Engineering, National University of Singapore, Singapore 117576, Singapore. Tel.: +65 65164272; fax: +65 67730339.
E-mail address: bieliaos@nus.edu.sg (S. Liao).

1742-7061/$ - see front matter
doi:10.1016/j.actbio.2007.03.007

After cross-linking the peptide–amphiphile fibers, Stupp et al. were able to direct mineralization of hydroxyapatite (HA) to form a composite material in which the crystallographic c-axes of HA were aligned along the long axes of the fibers. This alignment is similar to that observed between collagen fibrils and HA crystals in natural bone [4]. However, this model does not simulate higher-level assembly. Because the micro–macro hierarchical structure is not modeled, it is not possible to infer realistic gross mechanical properties.

Since the discovery of fullerenes and carbon nanotubes, the unique structure-dependent electrical and mechanical properties of carbon structures have been the subject of extensive research [9]. Potential applications include nanodevices, nanosensors, ultra-high-strength engineering fibers, etc. To optimize the use of carbon nanotubes (CNTs) in these applications, a number of strategies have also been developed for the surface modification of CNTs by functional groups and functional-group-anchored nanoparticles [10–12]. It has demonstrated that open-ended single-walled carbon nanotubes (SWCNTs) can be solubilized in organic solvents, and can be further derivatized by the adsorption of hydroxystilbene fluorophore onto the carbon surface via ester coupling [12]. Mixed-monolayer-protected Au clusters can be strongly adsorbed onto the carbon surface. SWCNTs that are prepared via alumina-membrane synthesis and filled Pt/Ru nanoparticles can act as an electrocatalyst for methanol oxidation and oxygen reduction [13]. Han et al. reported a simple and effective method for preparing alkanethiolate monolayer-capped gold nanoparticles on multi-walled carbon nanotubes (MWCNTs) by molecularly mediated assembly [14]. In yet another demonstration of the self-assembly capability of CNTs, Rosca et al. [15] and Li et al. [16] showed that after prolonged nitric acid oxidation, the fragmented MWCNTs aligned themselves into areas of parallel nanotubes, and had the tendency to self-organize into aligned nanotube ribbons. There has also been a tremendous interest in taking advantage of the unique properties of CNTs for promising biological applications. MWCNTs are capable of being shaped into three-dimensional (3-D) architectures, giving rise to the possibility of using this material as a new form of scaffold for tissue engineering [17]. In view of the high surface area/volume ratio, structure periodicity and molecular affinity, we studied the feasibility of using MWCNTs as a template for the fabrication of assembled nanohydroxyapatite (nHA). A comparison of the mechanism of mineralization of this template with the mineralization of collagen fibers may help develop a more rational design strategy for biomimetic materials for hard tissue repair. We hypothesize that the unique microstructure of certain MWCNTs with bamboo periodicity can direct the nanosized apatite assembly via an aqueous solution reaction. The dislocations on the surface of these CNTs can serve as sites for nucleation of HA after the MWCNTs are functionalized by carboxyl groups or other groups for calcium chelation [15,18–20]. We also compare the mechanism of in vitro mineralization of the collagen fibril unit with that of CNTs with and without carbonate. By studying the capability of CNTs to promote assembly and mineralization, it is possible to gain insights in new self-assembling mineralization systems.

2. Materials and methods

Non-carbonated nHA and carbonated nHA were prepared for comparative studies using MWCNTs and collagen as nucleation templates. MWCNTs with bamboo structures provided by Nanolab Inc. (USA) as shown in Fig. 1a were grown by chemical vapor deposition. They have a diameter of 20–40 nm, and an average length of 5.0 μm. The purification procedure for MWCNTs was as follows: First, MWCNTs were heated to approximately 773 K for 90 min under atmospheric conditions. Next, the cooled MWCNTs were transferred into a flask containing 6 M HCl and treated at 333 K for 2 h to remove residual metals and metal oxides. The acid solution was filtered using a polytetrafluoroethylene membrane filter with a pore size of 0.2 μm. The filtered cake was rinsed out with double-distilled water and subsequently dried at 333 K for 12 h.

The above-purified MWCNTs were added to 0.5 M acetic acid. Solutions of 0.5 M $CaCl_2$ and 0.5 M H_3PO_4 (Ca/P = 1.66) were gradually added through separate tube pumps and the mixture stirred for 1 h. The mixture was then separated into two equal portions. A solution of Na_2CO_3 (molar ratio of $CO_3^{2-}/PO_4^{3-} = 3$) was gradually added to one of these portions. Both portions were stirred for 30 min, and then titrated with sodium hydroxide to pH 9 at room temperature [21]. After aging the solution for 2 h, two types of materials, namely nHA/MWCNTs (nHAM) and nano-carbonated HA/MWCNTs (nCHAM) were harvested from each of the portions by centrifugation and freeze-drying.

The above process was repeated with type I atelocollagen gel (2 wt.%, Koken Company, Japan) to make nHA/collagen (nHAC) and nano-carbonated HA/collagen (nCHAC) in a similar manner.

X-ray diffraction (XRD) analysis was performed in a Rigaku/Multiflex diffractometer using Ni-filtered Cu Kα radiation, in the 2θ range of 10°–80° at a scan rate of $2^\circ\ \mathrm{min}^{-1}$, with a sampling interval of 0.02°. Data were analyzed by the accompanying MDI JADE6 software [22]. The diffraction peak broadening due to small crystallites can be semi-quantitatively estimated from the Scherrer equation: $\beta_{1/2} = (K\lambda)/(D\cos\theta)$ [23]. $\beta_{1/2}$ is the full-width at half maximum in 2θ and this is automatically calculated by the MDI JADE6 software. K is a constant that we set to 1, λ is the X-ray wavelength in Angstroms, D is roughly the average crystallite size and the θ is the diffraction angle of the corresponding reflex.

A Raman spectrometer (Dilor Jobin Yvon Spex, Group Horiba) was also used to evaluate the samples.

The carbonated weight percentages were measured using thermogravimetric analysis (TGA) (Rigaku Thermoflex

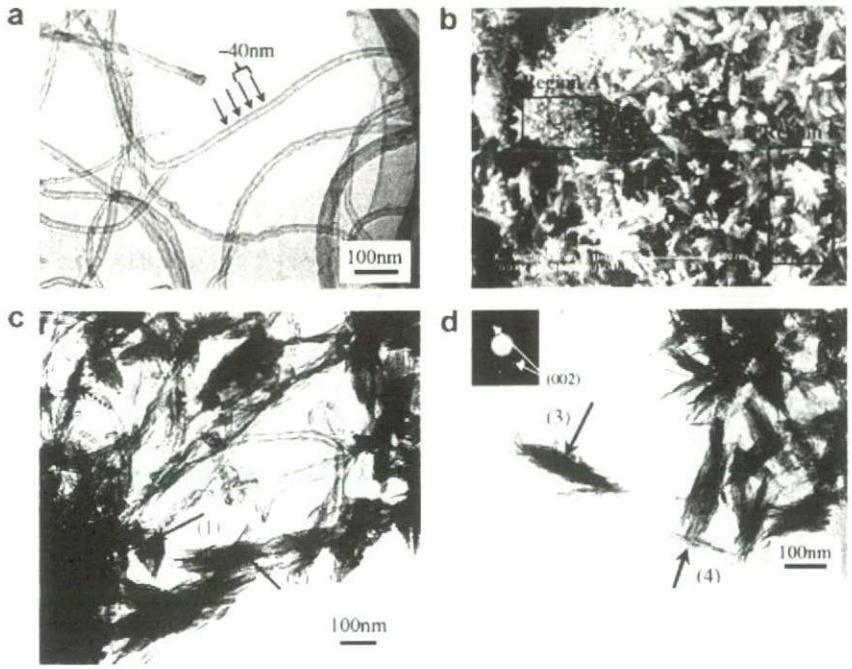

Fig. 1. (a) TEM of nanoscale bamboo structure in MWCNTs. The periodic structure of the bamboo is about 39.6 ± 11.8 nm ($n = 5$). (b) SEM micrographs of nHAM. The spindle unit is about 300 nm long. (c) Network of MWCNTs with nHA shown in region A of (b). Arrows 1 and 2 refer to the nHA attached to MWCNTs, arrow 2 denotes a relatively large nHA spindle unit. Dashed arrows refer to a small nHA spindle unit. (d) TEM analysis of area corresponding to region B in (b). Arrow 3 shows assembly of pure nHA and arrow 4 shows a small spindle unit of nHA. Arrows 2 and 3 indicate the same level spindle unit of nHA crystals. SAED of arrow 3 referring to a bundle of apatite is shown at the top left corner. This SAED demonstrates the orientation of the nHA phase.

TG8110/TAS100). Samples were heated at room temperature to a maximum temperature of 1000 °C at a heating rate of 10 °C min^{-1}. As in natural bone, the weight percentage of water content, organic material (mostly collagen), carbonated apatite and residual mineral (calcium phosphate) of the sample can be determined by the three stages of weight loss during the heating process [24,25].

To prepare samples for transmission electron microscopy (TEM), a drop of the aged reaction solution prior to the freeze-drying step was placed on a carbon film-supported copper grid. After air-drying, the sample was observed on a Hitachi-800 microscope at 150 kV. The freeze-dried samples after gold coating were observed by field emission scanning electron microscopy (FESEM) (Sirion 200, FEI Company, Delaware, USA).

3. Results

The periodic length of a typical MWCNT is approximately 40 nm (Fig. 1a). SEM micrograph observations (Fig. 1b) showed that assembled nHA was associated with MWCNTs. In general, the nHA was self-assembled into spindle-shaped units (Fig. 1b–d) of varying sizes. For example, the spindle-shaped units in region A of Fig. 1b are much smaller than the spindle-shaped units in region B. It is also observed that those spindle-shaped units that are still attached to MWCNTs (dashed arrow in Fig. 1c) are smaller than those that are detached from the MWCNTs (Fig. 1d, arrow 3). Occasionally, smaller spindle-shaped units were observed to be detached from MWCNTs (Fig. 1d, arrow 4). Selected area electron diffraction (SAED) of the apatite domain (Fig. 1d, arrow 3, referring to the apatite bundle) revealed that the spindle-shaped units were oriented in the same direction as the *c*-axes of nHA. This is highly suggestive that the spindle-shaped units are formed from an assembly of near-parallel nHA polycrystal fibril. In general, the spindle-shaped units that are detached from MWCNTs are larger than those spindle-shaped units that are still attached to MWCNTs. The initiation and crystallization phases are continuous processes, which start and terminate randomly at the different sites, and result in spindle-shaped units that vary in size from different regions depending on the local conditions. The detached spindle-shaped units are not only larger but also tend to be more uniform in size.

In this case, the spindle-shaped units tend to orient at an angle of 45° (44.8 ± 3.2°, $n = 5$) with respect to the longitudinal axis of the MWCNTs (Fig. 2a and b). The HRTEM image of the HA crystal on the surface of the MWCNTs revealed an apatite lattice spacing of 0.344 nm, corresponding to the (002) lattice plane of HA (Fig. 2b). As such, the angle between the MWCNT longitudal direction (white arrow) and the formed nHA *c*-axis (black arrow of crystal 1) was about 45° in this position. The three nHA crystals (1, 2 and 3) in Fig. 2b indicated that each nHA fibril was in a polycrystalline phase consisting of many connected small nHA crystals (Fig. 2a). Crystals 2 and 3 showed different directions to crystal 1 as denoted by the black

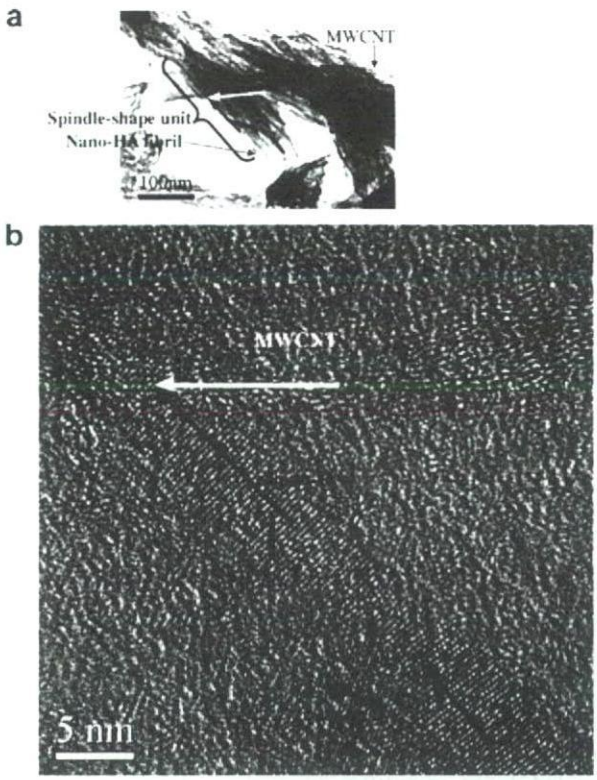

Fig. 2. Directional relationship of nHA and MWCNTs. HA polycrystal fibrils are arranged in parallel to form spindle-shape units that are oriented at an angle relative to the longitudinal axis of CNTs. The white arrow refers to the longitudinal direction of the MWCNTs; the black arrow refers to the orientation of the long axis of nHA [002]. (a) TEM image from Fig. 1c. (b) HRTEM image of nHA/MWCNT. The crystal lattice spacing was 0.344 nm, corresponding to the (002) surface of HA. The angle between the nHA and the MWCNTs was about 45°. Nos. 1, 2 and 3 indicate three HA nanocrystals, as part of a nHA polycrystal fibril.

arrows. This interpretation is also consistent with the typical SAED pattern in Fig. 1d.

A comparison between nHA derived from collagen templates and those derived from MWCNT templates revealed that low-level assemblies consisting of spindle-shaped units were similar in size and shape (Fig. 3a and b). Typically, these spindle-shaped units are more than 300 nm in length and about 60 nm in width. This microstructure may be due to the over-growth of HA on the templates (collagen or MWCNTs) provided that there is sufficient space for continuous growth.

Carbonate can be incorporated into nHA using the biomimetic method described here. The XRD spectra (Fig. 4) showed that all four materials (nHAC, nHAM, nCHAC and nCHAM) were nHA, except for nHAM, which contained micrometer levels of brushite impurities. Brushite is not usually seen when collagen is used as a template because the abundance of nucleation sites and the spatial structure of collagen molecules limit excess growth of nHA and brushite formation. Using software to calculate the peak of [002] in the X-ray data spectra, the average crystal size of each material (nHAM, nCHAM, nHAC, nCHAC) was 41.93 ± 4.70, 16.32 ± 2.92, 26.61 ± 16.33 and 11.61 ± 0.52 nm, respectively. Without the addition of carbonate during preparation, nHAM and nHAC both produced an apatite phase that was larger than those in nCHAM and nCHAC. This is consistent with the TEM observations. From the TEM results (data not shown), the carbonated nHA in nCHAC and nCHAM in general are less than 100 nm in length. The carbonated nHA

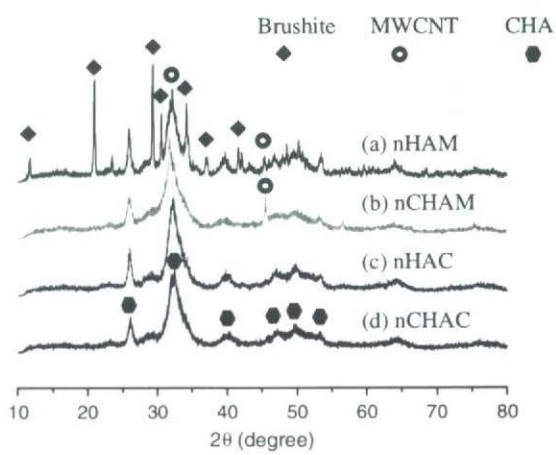

Fig. 4. XRD spectra of (a) nHAM, (b) nCHAM, (c) nHAC and (d) nCHAC. Except for (a), the others are nano-carbonated HA phase without any impurities. (a) is nano-carbonated HA with brushite. From the calculation of the peak of [002] in the spectra, the HA average crystal size for each material was 41.93 ± 4.70, 16.32 ± 2.92, 26.61 ± 16.33 and 11.61 ± 0.52 nm, respectively. The carbonated HA phases in (b) and (d) were both smaller than those of (a) and (c).

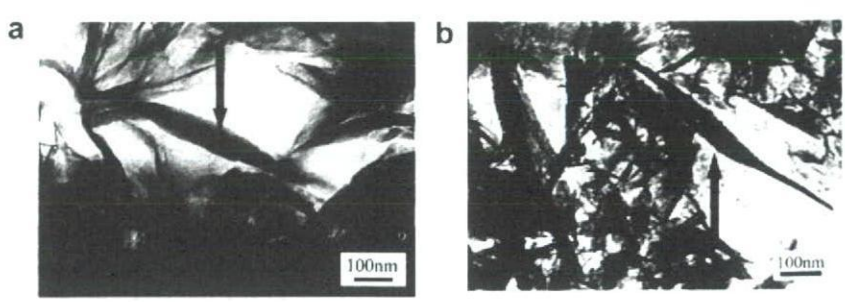

Fig. 3. Spindle-shaped units of apatite co-precipitated with (a) collagen and (b) MWCNTs are of similar size. Each unit is greater than 300 nm in length and 60 nm in width.

(nCHAC and nCHAM) is relatively smaller than the non-carbonated nHA (nHAC and nHAM). In addition to reducing crystal size, carbonation also causes a reduction in tendency to self-assemble into spindle-shaped units, especially when mineralization is carried out with MWCNTs. As a result, only a few of the nCHAC polycrystal fibrils were oriented in a parallel fashion, and in nCHAM there was no distinctive parallel orientation of the polycrystal fibrils. TGA results showed that the carbonate content found in the four materials (nHAM, nCHAM, nHAC, nCHAC) was 4.9%, 7.1%, 4.8% and 7.1%, respectively. The detection of carbonate in nHAM and nHAC is probably due to the absorption of atmospheric carbonate during the preparation process. These results also mean that a slight increase in carbonate content in the composites is associated with a significant decrease in the crystal size regardless of the type of template used.

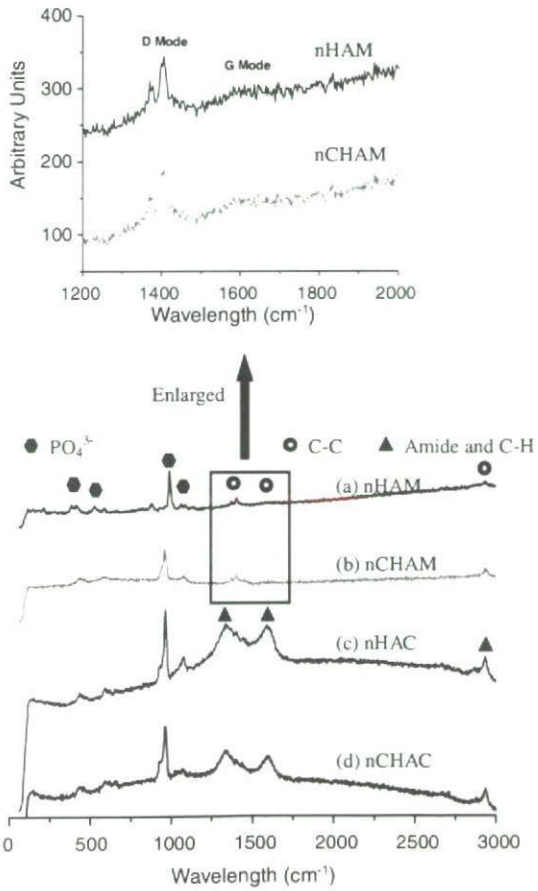

Fig. 5. Raman Spectra of (a) nHAM, (b) nCHAM, (c) nHAC and (d) nCHAC. After replacing MWCNT with collagen, the distinct peaks of amide and C–H were seen. Phosphate was seen in all four spectra, but the phosphate bands in (c) and (d) were higher than those in (a) and (b). In the enlarged portion of (a) and (b), D and G modes are indicated in the upper part of spectra. This is a significant D-mode peak consisting of two sub-peaks. Comparing D-mode peaks of (a) and (b), peaks did not shift significantly (about 1405.775–1370.592 cm^{-1}), and hence this was assigned as the disorder-induced D mode. The D-mode peak is attributed to a finite particle size effect or lattice distortion, such as defects in the curved graphite sheets, tube ends or bamboo structures. On the other hand, the G mode in the two spectra did not show any significant peaks, which is a characteristic of graphite sheets.

In order to detect the interaction between the templates and nHA, we compared the four composites by Raman spectroscopy (Fig. 5). In the enlarged portion of the graph for nHA prepared with MWCNTs, the D and G modes are shown. The D mode has a significant peak, which is made up of two sub-peaks. Comparing the D mode of nHAM and nCHAM, there was no significant shift in the peaks (from 1406 to 1370 cm^{-1}), and hence this was assigned as the disorder-induced D mode. The D-mode peak is attributed to a finite particle size effect or lattice distortion, such as defects in the curved graphite sheets, tube ends or finite size crystalline domains in the nanotubes (nanobells or bamboo structures), etc. [26,27]. The G mode in both spectra occurred at about 1600 cm^{-1}. The G mode also did not display any obvious peaks, which is a characteristic of graphite sheets. However, after replacing MWCNT templates with collagen, distinct peaks of amide and C–H were observed in the spectra.

4. Discussion

It is demonstrated that nucleation and growth of nHA can be initiated by MWCNTs. Raman spectra of nHAM revealed large quantities of surface defects around the MWCNTs. HRTEM of MWCNTs reveals a class of defects analogous to edge dislocation in a crystal [28]. These defects are sites for nucleation and growth of nHA crystals. We suspect that when the aggregations of nHA polycrystal fibril forming the spindle-shaped units reach a sufficient size, these spindle-shaped units become more susceptible to detachment from the MWCNTs. Such speculation is consistent with the observation that detached spindle-shaped units tend to be larger. As a result, we postulate that once the spindle-shaped units have reached a sufficient size, they are detached from the MWCNTs, possibly due to the agitation from stirring, and once detached, the assembly process terminates.

Some investigators reported that several weeks are required for sufficient mineralization to occur if simulated body fluid (SBF) or modified SBF is used [8,29]. There is no apatite formation with CNTs using standard SBF or PBS unless F ions are added and the phosphate concentration is increased [30]. These findings are analogous to our experience that CNTs are not as strong a template as collagen in inducing formation of nHA crystals. However, in the method described here, using a mixture of calcium, phosphate and carbonated ions, mineralization can be achieved in less than a day.

In natural bone, collagen fibrils consist of self-assembled collagen triple helices. Along the long axis of collagen, the quarterly staggered pattern produces a 67 nm long periodic structure with 40 nm hole and 27 nm folded part. The holes provide sites for mineral nucleation and growth. Minerals assemble along the long axis and contiguous channels allow for the creation of 3-D layers in natural mineralized

tissue [1,2,31]. Our previous in vitro collagen mineralization experiment showed that HA crystals could also nucleate and grow on the surface of collagen fibrils. Previous studies have proven that the negatively charged carboxyl and carbonyl groups found in collagen molecules can act as nucleation sites for HA crystals [32]. This is because oxygen in the hydroxyl group of HA has an epitaxial relationship with the carboxyl groups of collagen. Furthermore, HA crystals covering the surface of collagen fibrils were observed to have their *c*-axes aligned along the longitudinal axes of collagen fibrils. These mineralized collagen bundles were assembled from parallel collagen fibers with calcium phosphate crystals on their surfaces. In an analogous manner, physical and chemical treatments can be employed to align HA crystals. One such method is to add carboxyl or carbonyl functional groups to CNTs so that CNTs possess both structural compatibility and chemical complementarity for mineral formation. Based on such a complimentary and directional relationship between CNTs and apatite, a novel method was used to induce apatite assembly. We speculate that compared to collagen, MWCNTs are a less ideal template for nucleation and growth of the nHA and, as a result, brushite is formed as a by-product. This undesirable by-product can be eliminated by the addition of carbonate. In addition to the special spatial structure of the CNT surface, it is possible that the oxidation of the CNT surface to carboxylic group can also enhance the nucleation of nHA. Comparison of the relative peak ratio in the Raman spectra has shown that MWCNTs contribute about 0.18 wt.% to the composites, and this is much lower than the collagen content (16.5 wt.%) for composites using collagen as a template. Despite the small percentage of templates, MWCNTs are a productive template for HA crystal formation. This is due to their large surface area (220 $m^2 g^{-1}$) with abundant defects acting as mineral nucleation sites for HA crystallization. Moreover, the 40 nm periodic bamboo structure provides the periodic defect structure on the surface of CNTs for nucleation sites of HA. In this study, we control the size of formed HA by controlling the time of the reaction. If MWCNTs are further assembled into an aligned array, the space between parallel CNTs will limit the over-growth of HA, as occurs in the collagen assembly of natural bone tissue. The hierarchical assembly of MWCNTs with HA can thus be recognized as being similar to natural mineralized tissue.

In conclusion, the proposed process of apatite assembly is summarized schematically in Fig. 6. The multi-walled surfaces of the nanotubes provide abundant sites for the nucleation of apatite in the solution. A single unit of the bamboo structure was used as an example to illustrate the mineralization process. The carboxylic groups on the surface act as the coordination bonds for chelation of calcium in HA crystals. The nucleated apatite temporarily attaches along the interface of carbon layers (Fig. 6b). Moreover, the growing apatite crystals can be easily detached from the MWCNTs (Fig. 6c) due to weak functionalization of the binding groups and the unstable support of the growing apatite crystals on the curved surface of the MWCNT. The nHA polycrystal fibrils are assembled into a parallel array of spindle-shaped units. When the apatite assembly unit reaches a sufficient size, it separates from the carbon nanotubes probably due to the pertubation from stirring. This exposes the surface of the MWCNTs for further nucleation (Fig. 6a).

This separated spindle-shaped unit can be used as the building block for assembling high-level biomaterials. An important application is the development of substitute material for hard tissue using this biomimetic method. For example, enamel is a hard, wear-resistant material with highly ordered micro/nano architecture consisting of carbonated HA crystallites assembled into a woven prism structure. Organic matrix components make up less than 2% of the enamel [5,6]. Unlike bone tissues, enamel does not contain collagen and does not undergo remodeling. On the other hand, 60% of the underlying dentine consists

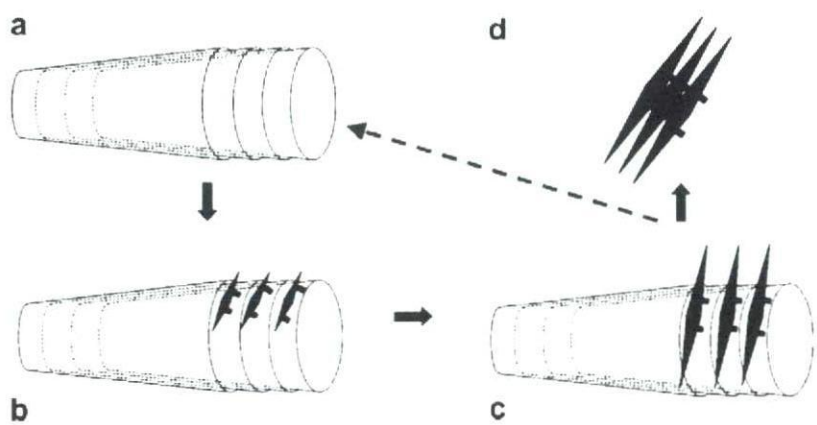

Fig. 6. Schematic illustration of the assembly process of HA on MWCNTs. (a) Bamboo unit of the MWCNTs. (b) The nucleation of HA on the surface of CNTs. (c) The growth of the HA fibrils occurs on the surface of the CNTs. The HA fibrils are oriented parallel to each other and assemble into a spindle unit. (d) The assembled HA dissociates from the MWCNTs, leaving an open site for formation of new HA if sufficient calcium and phosphate ions are present in the solution. Red rods refer to the chemical functional bonds and blue prisms refer to nHA polycrystal fibril. (For interpretation of the references to colour in this figure legend, the reader is referred to the web version of this article.)

of mineral crystals, which grow in the gaps between staggered or overlapped collagen fibrils. Until now, there has been no effective method for the preparation of hierarchical materials such as enamel and dentine. The nanoscale similarity between nHA assembled on MWCNTs and natural enamel tissue opens the possibility of fabricating biomimetic materials similar to natural tooth. In view of previously unsuccessful attempts to mimic the hierarchical structure of enamel on the nanometer and micrometer scales [33], carbon nanotubes may provide a promising platform for further research in the systematic incorporation and assembly of organic, inorganic and biological composites in a template for nucleation, growth and alignment over multiple length scales. Therefore, future work will be focused on the high-level self-assembly of functionalized MWCNTs and HA, which could lead to a more complete imitation of natural hard tissue.

Acknowledgements

This work was supported in part by the JSPS Program in Japan, the 2002–2005 Health and Labor Sciences Research Grants for Research on Advanced Medical Technology: "Tissue Reaction and Biomedical Application of Nanotubes, Nanoparticles and Microparticles (H14-Nano-021)" from the Ministry of Health, Labor, Sports and Welfare, Japan, and NUS LKY PDF fellowship in Singapore.

References

[1] Landis WJ, Song MJ, Leith A. Mineral and organic matrix interaction in normally calcifying tendon visualized in three dimensions by high-voltage electron microscopic tomography and graphic image reconstruction. J Struct Biol 1993;110:39–54.
[2] Lowenstam HA, Weiner S. On biomineralization. New York: Oxford University Press; 1989. p. 35–40.
[3] Zhang S. Fabrication of novel biomaterials through molecular self-assembly. Nat Biotechnol 2003;21:1171–8.
[4] Hartgerink JD, Beniash E, Stupp SI. Self-assembly and mineralization of peptide-amphiphile nanofibers. Science 2001;294:1684–8.
[5] Du C, Falini G, Fermani S, Abbott C, Moradian-Oldak J. Supramolecular assembly of amelogenin nanospheres into birefringent microribbons. Science 2005;307:1450–4 [Erratum: Science 2005; 309:2166].
[6] Moradian-Oldak J, Du C, Falini G. On the formation of amelogenin microribbons. Eur J Oral Sci 2006;114:289–96.
[7] Arthur V. A window on biomineralization. Science 2005;307:1419–20.
[8] Murphy WL, Mooney DJ. Bioinspired growth of crystalline carbonate apatite on biodegradable polymer substrata. J Am Chem Soc 2002;9:1910–7.
[9] Iijima S. Helical microtubules of graphitic carbon. Nature 1991;354:56–8.
[10] Sun YP, Huang W, Lin Y, Fu K, Kitaygorodskiy A, Riddle LA, et al. Soluble dendron-functionalized carbon nanotubes: preparation, characterization, and properties. Chem Mater 2001;13:2864–9.
[11] Jiang K, Eitan A, Schadler LS, Ajayan PM, Siegel RW. Selective attachment of gold nanoparticles to nitrogen-doped carbon nanotubes. Nano Lett 2003;3:275–7.
[12] Djalali R, Chen YF, Matsui H. Au nanocrystal growth on nanotubes controlled by conformations and charges of sequenced peptide templates. J Am Chem Soc 2003;125:5873–9.
[13] Che G, Lakshmi BB, Fisher ER, Martin CR. Carbon nanotubule membranes for electrochemical energy storage and production. Nature 1998;393:346–9.
[14] Han L, Wu W, Kirk Louis F, Luo J, Maye MM, Kariuki NN, et al. A direct route toward assembly of nanoparticle-carbon nanotube composite materials. Langmuir 2004;20:6019–25.
[15] Rosca ID, Watari F, Uo M, Akasaka T. Oxidation of mutiwalled carbon nanotubes by nitric acid. Carbon 2005;43:3124–31.
[16] Li YH, Xu C, Wei B, Zhang X, Zheng M, Ajayan PM. Self-organized ribbons of aligned carbon nanotubes. Chem Mater 2002;14:483–5.
[17] Correa-Duarte MA, Wagner N, Rojas-Chapana J, Morsczeck C, Thie M, Giersig M. Fabrication and biocompatibility of carbon nanotube-based 3D networks as scaffolds for cell seeding and growth. Nano Lett 2004;4:2233–6.
[18] Yu ZH, Brus LE. Reversible oxidation effect in Raman scattering from metallic single-wall carbon nanotubes. J Phys Chem 2000;A104: 10995–9.
[19] Kuznetsova A, Popova I, Yates JT, Bronikowski MJ, Huffman CB, Liu J, et al. Oxygen-containing functional groups on singlewall carbon nanotubes: NEXAFS and vibrational spectroscopic studies. J Am Chem Soc 2001;123:10699–704.
[20] Kukovecz A, Kramberger C, Holzinger M, Kuzmany H, Schalko J, Mannsberger M, et al. On the stacking behavior of functionalized single-wall carbon nanotubes. J Phys Chem 2002;B106:6374–80.
[21] Liao S, Watari F, Uo M, Ohkawa S, Tamura K, Wang W, et al. The preparation and characteristics of a carbonated hydroxyapatite/collagen composite at the room temperature. J Biomed Mater Res 2005;74B:817–21.
[22] MDI JADE6 software, XRD pattern processing. Materials Data, Inc.; 2003.
[23] Klug HP, Alexander LE. X-ray diffraction procedures for polycrystalline and amorphous materials. New York: Wiley Interscience; 1974.
[24] Suchanek WL, Shuk P, Byrappa K, Riman RE, TenHuisen KS, Janas VF. Mechanochemical-hydrothermal synthesis of carbonated apatite powders at room temperature. Biomaterials 2002;23:699–710.
[25] Peters F, Schwarz K, Epple M. The structure of bone studied with synthrotron X-ray diffraction, X-ray absorption spectroscopy and thermal analysis. Thermochim Acta 2000;361:131–8.
[26] Zhang GY, Ma XC, Zhong DY, Wang EG. Polymerized carbon nitride nanobells. J Appl Phys 2002;91:9324–32.
[27] Wang YY, Tang GY, Koeck FAM, Brown B, Garguilo JM, Nemanich RJ. Experimental studies of the formation process and morphologies of carbon nanotubes with bamboo mode structures. Diam Relat Mater 2004;13:1287–91.
[28] Gerard Lavin J, Subramoney S, Ruoff RS, Berber S, Tomanek D. Scrolls and nested tubes in multiwall carbon nanotubes. Carbon 2002;40:1123–30.
[29] Rhee SH, Lee JD, Tanaka J. Nucleation of hydroxyapatite crystal through chemical interaction with collagen. J Am Ceram Soc 2000;83:2890–2.
[30] Akasaka T, Watari F, Sato Y, Tohji K. Apatite formation on carbon nanotubes. Mater Sci Eng C 2006;26:675–8.
[31] Holmes DF, Graham HK, Trotter JA, Kadler KE. STEM/TEM studies of collagen fibril assembly. Micron 2001;32:273–85.
[32] Zhang W, Huang KL, Liao SS, Cui FZ. Nucleation sites of calcium phosphate crystals during collagen mineralization. J Am Ceram Soc 2003;86:1052–4.
[33] Du C, Moradian-Oldak J. Tooth regeneration: challenges and opportunities for biomedical material research. Biomed Mater 2006;1:R10–7.

Effect of carbon nanotubes on cellular functions *in vitro*

Xiaoming Li,[1] Hong Gao,[2] Motohiro Uo,[1] Yoshinori Sato,[3] Tsukasa Akasaka,[1] Qingling Feng,[4] Fuzhai Cui,[4] Xinhui Liu,[5] Fumio Watari[1]

[1]*Department of Biomedical Materials and Engineering, Graduate School of Dental Medicine, Hokkaido University, Sapporo 060-8586, Japan*

[2]*Division of Applied Bioscience, Graduate School of Agriculture, Hokkaido University, Sapporo 060-8586, Japan*

AQ2 [3]*Graduate School of Environmental Studies, Tohoku University, Sendai 980-8579, Japan*

[4]*Department of Materials Science and Engineering, Key Laboratory of Advanced Materials, Tsinghua University, Beijing 100084, China*

[5]*Department of Orthopaedics, the First hospital of Hebei Medical University, Shijiazhuang 050031, China*

Received 11 March 2008; revised 20 June 2008; accepted 23 June 2008
Published online 00 Month 2008 in Wiley InterScience (www.interscience.wiley.com). DOI: 10.1002/jbm.a.32203

Abstract: Carbon nanotubes (CNTs) have been shown to affect cell behavior. But how and why the CNTs affect potential differentiation of the attached cells has not been largely known. In this study, multiwalled carbon nanotubes (MWNTs) and graphite (GP) were pressed as compacts. Higher ability of CNTs to adsorb proteins, compared with GP, was shown. Myoblastic mouse cells (C2C12) were cultured and the cell responses to the two kinds of compacts were compared *in vitro*. Meanwhile, we used cell culture on the culture plate as a control. During the conventional culture, significantly better cell attachment, proliferation, and differentiation of cells on the MWNTs were found. To confirm the hypothesis that the larger amount of protein adsorbed on the CNTs was crucial for this, we made the compacts adsorb more proteins in culture medium with 50% fetal bovine serum (FBS) before cell culture. With the adsorption of the proteins in advance, the increments of the total-protein/DNA and alkaline phosphatase (ALP)/DNA for the MWNTs was respectively as about 11 times and 18 times as the increments of those for GP and the control at both day 4 and day 7. Therefore, the CNTs might induce cellular functions by adsorbing more proteins, which indicated that the CNTs might be a candidate for scaffold material for tissue engineering. © 2008 Wiley Periodicals, Inc. J Biomed Mater Res 00A: 000–000, 2008

Key words: carbon nanotubes; cell differentiation; alkaline phosphatase (ALP); protein; tissue engineering

INTRODUCTION

The practice of using tissue engineering to repair tissue damages is attracting more and more attention.[1–7] Scaffolds, lying at the heart of all the new tissue engineering approaches, act as a substrate for cellular attachment, proliferation, and differentiation.[5–8] In the imminent ageing society of the 21st century, nanomaterials have been widely investigated for potential application in the medical field.[9,10] The nano-dimensionality of nature has logically given rise to the interest in using nanomaterials to prepare scaffolds for tissue engineering. These materials have the potential to have a significant impact on tissue engineering.[11–14] Carbon nanotubes (CNTs), one of the most representative nanomaterials, with unique electrical, mechanical, and surface properties, were first reported in the year of 1991 and up to now appear well suited as a biomaterial.[14–27]

Several studies have been carried out on the interaction between CNTs and a variety of cells including osteoblasts, showing CNTs to be excellent substrates for cellular attachment and growth.[28–36] But few (if any) studies have elucidated the effect of CNTs on the protein content and potential differentiation of the attached cells, although cell differentiation is also very important for tissue repair.[37–39]

To start the differentiation of cells, it has been suggested that nanostructures of the biomaterials are critical.[40–46] In other words, the microenvironment around the cells may be crucial.[45,46] Fujibayashi et al. suggested that even a nonsoluble metal that contains no calcium or phosphorus can be an osteoinductive material when treated to form an appropriate nanostructure.[41] Popat et al. presented osteogenic differ-

Correspondence to: X. Li; e-mail: x.li@den.hokudai.ac.jp
Contract grant sponsor: Japan Society for the Promotion of Science (JSPS)

J_ID: ZA1 Customer A_ID: 08-0205.R2 Cadmus Art: JBMA32203 Date: 30-JULY-08 Stage: I Page: 2

entiation of C57 BJ mice marrow stromal cells on nanoporous alumina surfaces, suggesting the ability of nanostructured biomaterials to enhance cell differentiation.[47] Yim et al. reported the nanopatterns, reproduced on poly (dimethylsiloxan) (PDMS) using soft lithography on the nanoimprinted poly (methyl methacrylate) (PMMA)-coated Si master mold, played an important role in directing differentiation of adult stem cells into neuronal lineage.[48]

In this study, myoblastic mouse cells (C2C12) were cultured on multiwalled CNTs (MWNTs) compacts, comparing on graphite (GP) compacts, with and without the adsorption of fetal bovine serum (FBS) in advance. Cell differentiation was examined and compared, as well as cell attachment and proliferation. Meanwhile, we used cell culture on the culture plate as a control.

MATERIALS AND METHODS

Materials

MWNTs used in this study were obtained from Nano-Lab (Brighton, MA). The MWNTs of curled shape with about 90 nm in diameter were produced by the chemical vapor deposition (CVD) method. The purification procedure for MWNTs was as follows: First, MWNTs were heated to ~500 C for 90 min under atmospheric conditions. Next, the cooled MWNTs were transferred into a flask containing 6*M* HCl and treated at 60 C for 2 h, and then washed thoroughly with deionized water and completely dried. The GP particles used in this study were about 4.5 μm in diameter.

Fabrication of compacts

MWCTs and GP with the same weight were separately compacted serially in a steel-tool die via a uniaxial pressing cycle (0.09 GPa for 2 min, then 0.22 GPa for 3 min, finally 0.36 GPa for 3 min) at room temperature. The compacts were washed ultrasonically with acetone, 70% ethanol, and RX-water for 15 min and then dried at 60 C. All the compacts were sterilized by ultraviolet radiation for 48 h prior to experiments with cells. The morphology of the compacts was examined by scanning electron microscopy (SEM; S-4000, Hitachi, Japan).

Evaluation of protein adsorption on the compacts

Before cells culture, ability to adsorb proteins of the compacts was evaluated. At first, 0.25% FBS (250 μL FBS in 100 mL 25 ppm NaN3 solution) were sterilized with 0.22 μm filter. After immersing the compacts respectively for 1, 4, and 7 days, the residual protein content (P_1) of the FBS solution (3 mL per sample, $n = 5$) was determined with the QuantiPro™ BCA Assay Kit (TaKaRa BIO INC, Japan) according to the guideline of the company. The fluorescence was measured with a BIO-TEK automate microplate reader at 620 nm. The adsorbed protein (P_a) was determined by the formula of $(0.25\% - P_1)/0.25\%$.

Conventional cell culture on the samples

The compacts were placed in the cell culture plates. Then C2C12 were respectively seeded on the compacts with a cell density of 2.0×10^4 per sample. Then the samples were put into an incubator at 37 C in a humidified atmosphere with 5% CO_2 and 95% air for 4 h. Finally, 2.5-mL culture medium, Dulbecco's modified Eagle's medium (DMEM; Sigma) with 10% fetal bovine serum (FBS; Biowest) and 1% penicillin/streptomycin (100 U/mL penicillin, 10 μg/mL streptomycin), was added into the walls of the plates and then, the plates were put back to the incubator. The culture mediums were refreshed twice a week.

SEM observation

At the prescribed time, the samples were rinsed with PBS to remove nonadherent cells, fixed in a solution of 2% glutaraldehyde, and postfixed in a 1% osmium tetroxide solution. Then, the samples were dehydrated in a series of solutions with increasing ethanol concentrations, followed by critical-point drying at 40 C. Finally, the morphology of the cells on the compacts was examined by SEM (S-4000, Hitachi, Japan).

DNA, ALP, and total protein analyses

After cell culture, the samples with cells were washed by PBS for three times after the cultured medium was totally removed. Then the samples were stored in the freezer at −80 C for at least 12 h for the biochemical analyses. As soon as the plates were taken out from the freezer, they were kept on the ice, prepared in advance. And then 0.5 mL 0.2% triton was put into each wall with samples in the plates. The plates were shook gently for 45 min. Finally, the solutions were analyzed for DNA, ALP, and protein content.

DNA content was determined with the CyQuant Cell Proliferation Assay Kit (Invitrogen) according to the guideline of the company. About 0.1 mL of each sample ($n = 4$) were diluted in TE to a final volume of 1.0-mL test tubes. Then 1.0-mL of aqueous working solution (dye) was added to each sample. After the tubes were incubated for about 3 min, the fluorescence using instrument parameters was measured at an emission wavelength of 520 nm and excitation of 480 nm. The DNA content of cells attached on the porous samples was counted through a premade standard DNA curve. DNA content was expressed as mean ± SD.

For the determination of ALP content, 20 μL of each sample ($n = 4$) was added to the walls of a 96-wall plate and then 100 μL Paranitrophenylphosphate (PNP) solution was added. After shaken gently, the plate was incubated at 37 C for 15 min. After 80 μL stop solution (0.2 mol/L sodium hydroxide) was added, the plate was read with a

ID: selvarajj Date: 30/7/08 Time: 19:14 Path: J:/Production/JBMM/VOL00000/080346/3B2/C2JBMM080346

J_ID: ZA1 Customer A_ID: 08-0205.R2 Cadmus Art: JBMA32203 Date: 30-JULY-08 Stage: I Page: 3

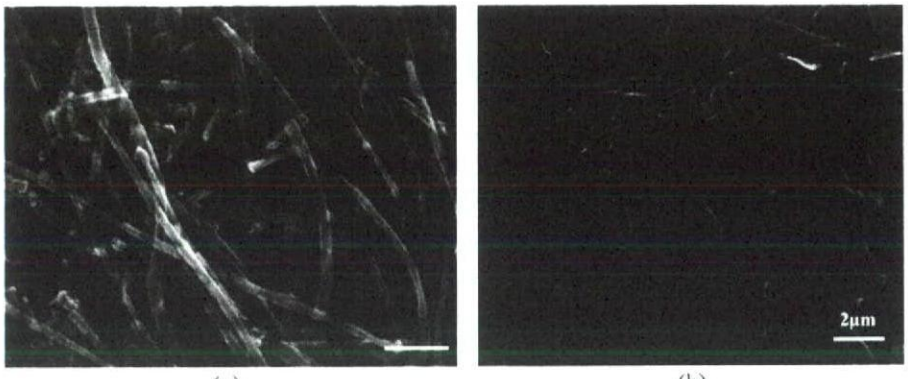

Figure 1. SEM images of the compacts: MWCNs (a); GP (b).

BIO-TEK automate microplate reader at 405 nm. For the standard curve, serial dilutions of p-Nitrophenol were made. Finally, the ALP content of cells was counted through the standard curve. The value was expressed as mean ± SD.

Total protein content was determined with the Quanti-Pro™ BCA Assay Kit (TaKaRa BIO INC). A total of 100 μL of each sample ($n = 4$) was added to the walls of a 96-wall and then 100 μL BCA solution was added. Then, the plate was continuously shaken for 2 h in dark at room temperature. Finally, the fluorescence was measured with a BIO-TEK automate microplate reader at 620 nm. The protein content, expressed as mean ± SD, was counted through a premade standard protein curve.

Cell culture on the samples after adsorbing FBS

At first, the samples were respectively immersed into culture medium containing 50% FBS for 24 h in an incubator at 37 C in a humidified atmosphere with 5% CO_2 and 95% air. Then, the FBS solution was completely removed and the discs were washed by the cultured medium of C2C12 with 1% FBS for three times. C2C12 was respectively cultured on the samples with a cell density of 4.0×10^4 per sample. After cell culture in culture medium with 1% FBS for certain time, DNA, ALP, and total protein content were examined with the methods mentioned above.

Statistical analysis

Statistical calculations were done with the SPSS (Chicago, IL) 12.0 software. Paired Student's *t*-test was used to analyze differences experiments results between different samples. $p < 0.05$ was regarded as significant difference.

RESULTS

The SEM images of the compacts were shown in Figure 1. The distinct difference in the structures between the MWNTs and GP compacts was exhibited. MWNTs formed a packed meshwork nanostructure, whereas GP compacts were formed with particles of about 4.5 μm. The ability to adsorb proteins of the compacts was showed in Figure 2, which showed that MWNTs compacts had much better ability to adsorb proteins than GP compacts. Although the mean value of the protein adsorption of GP compacts was greater than that of the culture plates (control), the statistical analysis showed that there was no significant difference between the two group values ($p > 0.05$).

Morphology of C2C12 cells cultured for 7 days on the compacts was shown in Figure 3. More cells could be observed on MWNTs than on GP compacts. Cells on MWNTs nearly grew to confluence after cultured for 7 days. For a comparison of cell attachment and proliferation at a quantitative stage, the results of DNA analysis of cells cultured on the different samples for 1, 4, and 7 days were shown in Figure 4. We used the slope of the curves in the

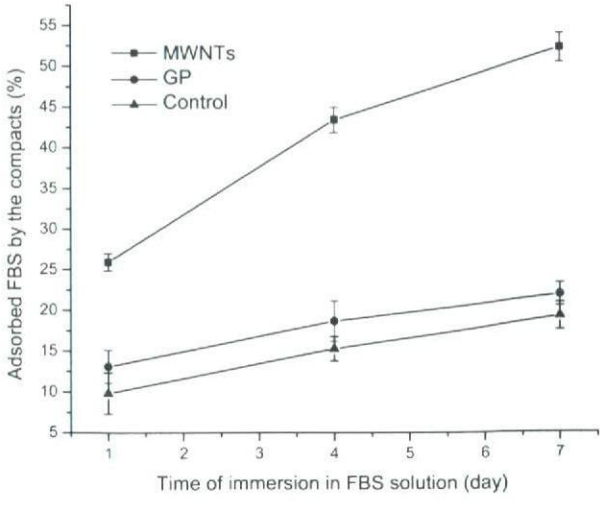

Figure 2. Protein adsorption of the samples ($n = 5$).

ID: selvarajj Date: 30/7/08 Time: 19:14 Path: J:/Production/JBMM/VOL00000/080346/3B2/C2JBMM080346

J_ID: ZA1 Customer A_ID: 08-0205.R2 Cadmus Art: JBMA32203 Date: 30-JULY-08 Stage: I Page: 4

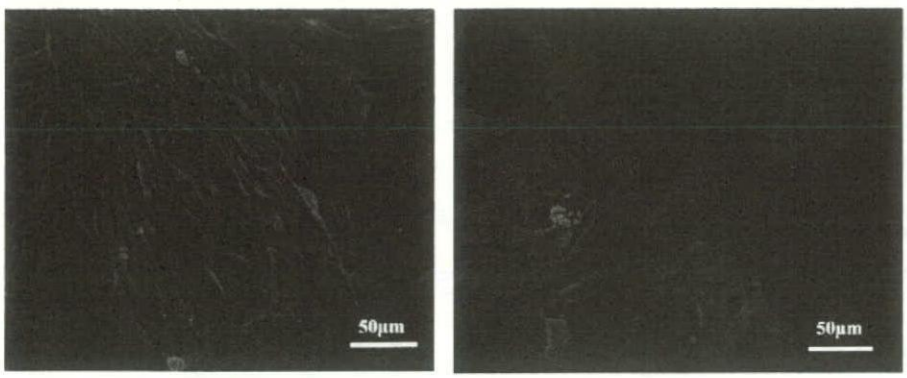

Figure 3. SEM images of cells conventionally cultured for 7 days on: MWNTs (a) and GP (b).

Figure 4 to estimate the cell proliferation, and thought that the difference in the DNA value at day 1 was mainly due to the different cell attachment. As shown in Figure 4, both the values at day 1 and the slope of the two curves are significantly greater, suggesting that C2C12 attach and proliferate better on MWNTs than on GP compacts (slop of the two curves from day 1 to day 4: 0.558 ± 0.022 vs. 0.219 ± 0.0155, $p < 0.01 < 0.05$; from day 4 to day 7: 0.489 ± 0.096 vs. 0.166 ± 0.0115, $p < 0.01 < 0.05$). Cell attached better on the plates (control) than on MWNTs, but no significant difference was found in the cell proliferation between on the plates and on the MWNTs (slop of the two curves from day 1 to day 4: 0.558 ± 0.022 vs. 0.563 ± 0.021, $p > 0.05$; from day 4 to day 7: 0.489 ± 0.096 vs. 0.468 ± 0.0311, $p > 0.05$), which might be because of the influence of the composition of the materials and the proteins adsorbed on the materials together.

F5 Figure 5 showed the results of ALP/DNA (alkaline phosphatase per unit cell). ALP/DNA of C2C12 cultured on MWNTs compacts was significantly higher than that on GP compacts and on the plates at each culture time point of 1, 4, and 7 days, whereas this value for GP compacts and control had no significant difference at each time point, suggesting that C2C12 differentiate toward osteogenic better on MWNTs than on GP and the plates. At day 7, the value for MWNTs was as about four times as that for GP and the control.

Total-protein/DNA (total protein content per unit cell) was showed in Figure 6. Total-protein/DNA of C2C12 cells on MMNTs was significantly higher than on GP and the culture plates at each culture time point of 1, 4, and 7 days. At day 7, the value for MWNTs was as about two times as that for GP. the Although the mean value of GP compacts was greater than that of the culture plates (control) at day 4 and 7, the statistical analysis showed that there was no significant difference between the two group values ($p > 0.05$). F6

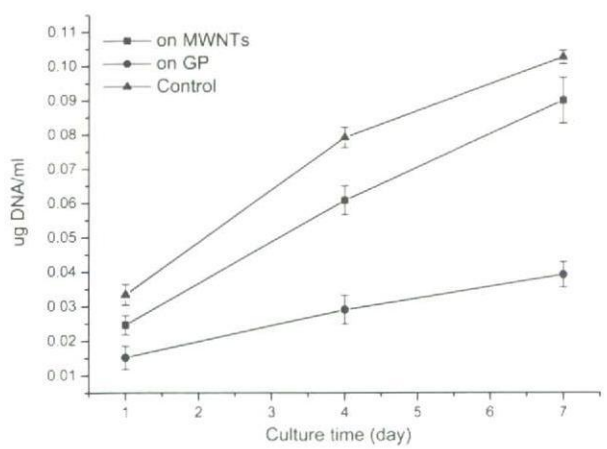

Figure 4. Results of DNA analysis of C2C12 cultured on samples ($n = 4$).

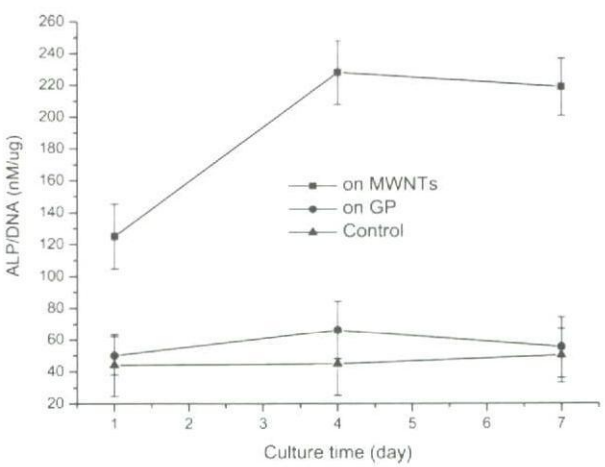

Figure 5. ALP/DNA of C2C12 cells conventionally cultured on samples ($n = 4$).

ID: selvarajj Date: 30/7/08 Time: 19:14 Path: J:/Production/JBMM/VOL00000/080346/3B2/C2JBMM080346

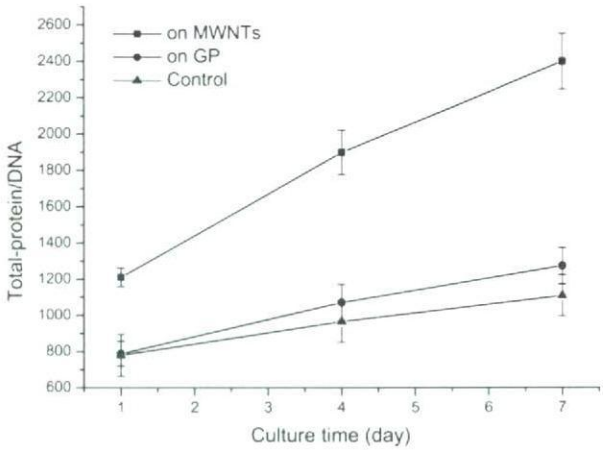

Figure 6. Total-protein/DNA of C2C12 cells conventionally cultured on samples ($n = 4$).

F7 Figure 7 showed ALP/DNA of C2C12 on the samples after adsorbing FBS at day 4 and day 7, compared with the results of the conventional cell culture. After the adsorption of FBS, ALP/DNA of cells on MWNTs increased significantly, while the value for GP increased slightly. The increased value for MWNTs was as about 18 times as that for GP and the control at both day 4 and day 7. The value for GP and the culture plates had no significant difference even after the adsorption of FBS ($p > 0.05$).

Total-protein/DNA of C2C12 on the samples after adsorbing FBS at day 4 and day 7, comparing with the results of the conventional cell culture, was F8 showed in Figure 8. Although the total-protein/DNA of cells on all the samples all increased after the adsorption of FBS, the value for MWNTs

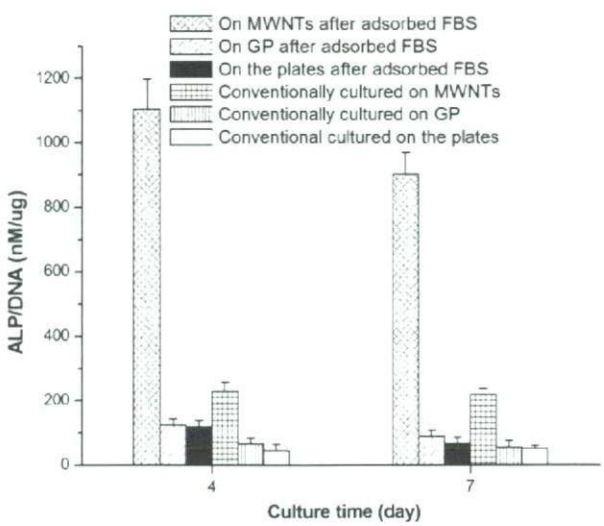

Figure 7. ALP/DNA of C2C12 cells cultured on samples with and without the adsorption of FBS in advance ($n = 4$).

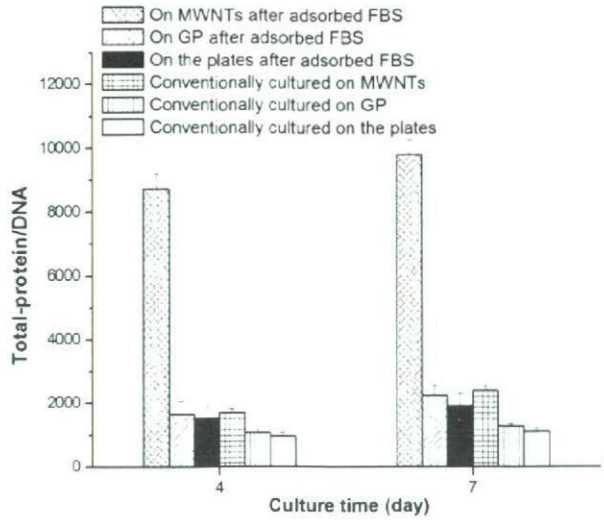

Figure 8. Total-protein/DNA of C2C12 cells cultured on samples with and without the adsorption of FBS in advance ($n = 4$).

increased most observably. The increased value for MWNTs was as about 11 times as that for GP and the control at both day 4 and day 7. The value for GP and the culture plates had no significant difference even after the adsorption of FBS ($p > 0.05$).

DISCUSSION

It has been previously reported that the biological response to implanted material is determined not only by its chemistry, but also by surface energy and topography.[46,49,50] Cells in their natural environment interact with extracellular matrix (ECM) components in the nanometer scale.[51,52] Logically, nanoscaled biomaterials should have positive effect on the cell functions.

We believe our study is the first time that C2C12 line, a multipotent cell line able to differentiate toward different phenotypes under the action of specific proteins, some chemical or biological factors, was cultured on the CNTs, and that not only cell attachment and proliferation, but also cell differentiation and cell activity were investigated. CNTs and GP are both isomorphs of pure carbon, composed of the same grapheme sheet structure. However, only CNTs have nanostructures. So in this study, comparison of the influence of CNTs and GP on C2C12 cells *in vitro* was done to figure out the effect of CNTs on cellular functions. Meanwhile, we used cell culture on the culture plate, which was made of polystyrene and tissue-culture treated, as a control.

The results showed that C2C12 attached and proliferated better on MWNTs than on GP. These results

J_ID: ZA1 Customer A_ID: 08-0205.R2 Cadmus Art: JBMA32203 Date: 30-JULY-08 Stage: I Page: 6

are consistent with what Aoki et al. have reported in their work, where they found osteoblasts attached and proliferated better on multiwalled and single-walled CNTs than on GP.[17,53] We think that in this study cells attachment and proliferation might be mainly influenced not only by the composition of the materials, but also by the proteins adsorbed on the materials together. Kilpadi et al. found that some specific proteins have different influence on human marrow stromal cells attachment and saos-2 osteosarcoma cells attachments on hydroxylapatite.[54] Since MWNTs compacts had higher ability to adsorb the proteins or higher affinities toward proteins than GP (Fig. 2), they should adsorb more proteins from the culture medium and these proteins might improve the attachment and proliferation of C2C12 cells.

Besides cell attachment and proliferation, cell differentiation should be most important evaluation point for biomaterials because it may directly contribute to the tissue repair. So in this study our focus has been mostly on this. Evaluating the proteins in cells may be an effective method to evaluate the differentiation. In this study, we used total-protein/DNA to evaluate the effect of MWNTs on the potential of the differentiation of per unit C2C12 cell. Meanwhile, we used the change in ALP/DNA of C2C12 cells to reify this effect. The technique, we used in this study for lysing cells before ALP, DNA, and protein analyses, has been confirmed that only cells, no adsorbed proteins, could be lysed from the samples in advance. From the results of conventional cell culture, we found that the ALP/DNA of C2C12 on MWNTs was significantly higher than on GP and the culture plates, suggesting that MWNTs induce this kind of cell to differentiate into osteogentic cells more than GP and culture plates. So, CNTs may be osteoinductive under certain circumstances. Some publications have shown that although with the same chemical composition, some materials are osteoinductive, some others are not.[46,55–57] These osteoinductive materials all have specific structures, indicating larger surface area and therefore higher ability to adsorb proteins. The work of Ripamonti and coworkers demonstrated that osteoinductivity in hydroxyapatite was linked to the precise shape of surface concavities in implants, which indicated a larger surface area, and that by using immunolocalization they demonstrated that this osteoinductivity occurred as a result of a concentration of specific proteins within the surface concavities.[58,59]

ALP is one kind of protein and only account for small ratio of total proteins in cells. So analyzing total proteins in cells may be an evaluation of the potential of cell differentiation into the expected cells. From the conventional cell culture in this study, we found that the total-protein/DNA C2C12 on MWNTs was significantly higher than on GP and the culture plates, which might suggest that MWNTs induce the potential differentiation of cells more than GP and culture plates. In other words, cells cultured on the MWNTs were more active.

So we hypothesized that the large amount of proteins adsorbed on the MWNTs played an important role in inducing cellular functions.

To confirm this hypothesis, we immersed the samples in culture medium containing 50% FBS to make them adsorb more proteins before cell culture. The results showed that after the adsorption of FBS, both the total-protein/DNA and ALP/DNA increased on all samples. Impressively, the value for MWNTs increased significantly most. The increments of the total-protein/DNA and ALP/DNA for MWNTs was respectively as about 11 times and 18 times as the increments of those for GP and the control at both day 4 and day 7. Therefore, the results of cell culture after the adsorption of FBS might be an effective proof for our hypothesis.

Hing[60] has reported that competitive protein adsorption at a bioactive surface may vary in three ways: (i) the quantity of protein adsorbed, (ii) the species of protein adsorbed, or (iii) the confirmation of the adsorbed protein. Also he supposed that nanostructures might thus influence protein adsorption by providing a larger surface area, thereby increasing the quantity of adsorbed growth factors above a critical level for cell recruitment and activation. In our study, we substantiated the importance of the protein adsorption. CNTs might adsorb large amount of proteins due to their larger surface area, unique electronic, catalytic, and chemical properties. These proteins might not only improve cell attachment and proliferation, but also be helpful for cell differentiation and therefore directly contribute to tissue repair.

CONCLUSION

It has been shown in this study that the CNTs could adsorb large amount of proteins, which might improve not only cell attachment and proliferation but also differentiation, which indicated that the CNTs might be a candidate for scaffold material for tissue engineering.

The authors acknowledge Dr. S. Abe and the graduate students in Department of Biomedical Materials and Engineering, Graduate School of Dental Medicine, Hokkaido University, Japan for their kind helps. Many thanks go to Dr. K. Wong of Cornell University for correcting English errors.

ID: selvarajj Date: 30/7/08 Time: 19:15 Path: J:/Production/JBMM/VOL00000/080346/3B2/C2JBMM080346

References

1. Capito RM, Spector M. Collagen scaffolds for nonviral IGF-1 gene delivery in articular cartilage tissue engineering. Gene Ther 2007;14:721–732.
2. Li XM, Feng QL, Liu XH, Dong W, Cui FZ. Collagen-based implants reinforced by chitin fibres in a goat shank bone defect model. Biomaterials 2006;27:1917–1923.
3. Spector M. Biomaterials-based tissue engineering and regenerative medicine solutions to musculoskeletal problems. Swiss Med Wkly 2006;136:293–301.
4. Li XM, Feng QL, Wang WJ, Cui FZ. Chemical characteristics and cytocompatibility of collagen-based scaffold reinforced by chitin fibers for bone tissue engineering. J Biomed Mater Res B 2006;77:219–226.
5. Spector M. Basic principles of tissue engineering. Tissue Eng 1999:3–16. AQ3
6. Li XM, Feng QL, Jiao YF, Cui FZ. Collagen-based scaffolds reinforced by chitosan fibres for bone tissue engineering. Polym Int 2005;54:1034–1040.
7. Ryu GH, Yang WS, Roh HW, Lee IS, Kim JK, Lee GH, Lee DH, Park BJ, Lee MS, Park JC. Plasma surface modification of poly (D,L-lactic-co-glycolic acid) (65/35) film for tissue engineering. Surf Coat Tech 2005;193:60–64.
8. Li XM, Feng QL. Porous poly-L-lactic acid scaffold reinforced by chitin fibers. Polym Bull 2005;54:47–55.
9. Labhasetwar V. What is next for nanotechnology? J Biomed Nanotechnol 2005;1:373–374.
10. Park GE, Webster TJ. A review of nanotechnology for the development of better orthopedic implants. J Biomed Nanotechnol 2005;1:18–29.
11. Watari F, Abe S, Koyama C, Yokoyama A, Akasaka T, Uo M, Matsuoka M, Totsuka Y, Esaki M, Morita M, Yonezawa T. Behavior of in vitro, in vivo and internal motion of micro/nano particles of titanium, titanium oxides and others. J Ceram Soc Jpn 2008;116:1–5.
12. Watari F, Yokoyama A, Omori M, Hirai T, Kondo H, Uo M, Kawasaki T. Biocompatibility of materials and development to functionally graded implant for bio-medical application. Compos Sci Technol 2004;64:893–908.
13. Yokoyama A, Sato Y, Nodasaka Y, Yamamoto S, Kawasaki T, Shindoh M, Kohgo T, Akasaka T, Uo M, Watari F, Tohji K. Biological behavior of hat-stacked carbon nanofibers in the subcutaneous tissue in rats. Nano Lett 2005;5:157–161.
14. Harrison BS, Atala A. Carbon nanotube applications for tissue engineering. Biomaterials 2007;28:344–353.
15. Mattson MP, Haddon RC, Rao AM. Molecular functionalization of carbon nanotubes and use as substrates for neuronal growth. J Mol Neurosci 2000;14:175–182.
16. Firkowska I, Olek M, Pazos-Perez N, Rojas-Chapana J, Giersig M. Highly ordered MWNT-based matrixes: Topography at the nanoscale conceived for tissue engineering. Langmuir 2006;22:5427–5434.
17. Aoki N, Yokoyama A, Nodasaka Y, Akasaka T, Uo M, Sato Y, Tohji K, Watari F. Strikingly extended morphology of cells grown on carbon nanotubes. Chem Lett 2006;35:508–509.
18. Correa-Duarte MA, Wagner N, Rojas-Chapana J, Morsczeck C, Thie M, Giersig M. Fabrication and biocompatibility of carbon nanotube-based 3D networks as scaffolds for cell seeding and growth. Nano Lett 2004;4:2233–2236.
19. Uo M, Tamura K, Sato Y, Yokoyama A, Watari F, Totsuka Y, Tohji K. The cytotoxicity of metal-encapsulating carbon nanocapsules. Small 2005;1:816–819.
20. Akasaka T, Watari F. Nano-architecture on carbon nanotube surface by biomimetic coating. Chem Lett 2005;34:826–827.
21. MacDonald RA, Laurenzi BF, Viswanathan G, Ajayan PM, Stegeman JP. Collagen-carbon nanotube composite materials as scaffolds in tissue engineering. J Biomed Mater Res A 2005;74:489–496.
22. Kam NWS, Jessop TC, Wender PA, Dai H. Nanotube molecular transporters: Internalization of carbon nanotube-protein conjugates into mammalian cells. J Am Chem Soc 2004;126:6850–6851.
23. Kam NWS, Liu Z, Dai H. Functionalization of carbon nanotubes via cleavable disulfide bonds for efficient intracellular delivery of siRNA and potent gene silencing. J Am Chem Soc 2005;127:12492–12493.
24. Supronowicz PR, Ajayan PM, Ullmann KR, Arulanandam BP, Metzger DW, Bizios R. Novel current-conducting composite substrates for exposing osteoblasts to alternating current stimulation. J Biomed Mater Res 2002;59:499–506.
25. Chen RL, Bangsaruntip S, Drouvalakis KA, Kam NWS, Shim M, Li Y. Noncovalent functionalization of carbon nanotubes for highly specific electronic biosensors. Proc Natl Acad Sci USA 2003;100:4984–4989.
26. Kiura K, Sato Y, Yasuda M, Fugetsu B, Watari F, Tohji K, Shibata K. Activation of human monocytes and mouse splenocytes by single-walled carbon nanotubes. J Biomed Nanotechnol 2005;1:359–364.
27. Sato Y, Yokoyama A, Shibata K, Akimoto Y, Ogino S, Nodasaka Y, Kohgo T, Tamura K, Akasaka T, Uo M, Motomiya K, Jeyadevan B, Ishiguro M, Hatakeyama R, Watari F, Tohji K. Influence of length on cytotoxicity of multi-walled carbon nanotubes against human acute monocytic leukemia cell line THP-1 in vitro and subcutaneous tissue of rats in vivo. Mol Biosyst 2005;1:176–182.
28. Pantarotto D, Briand J, Prato M, Pianco A. Translocation of bioactive peptides across cell membranes by carbon nanotubes. Chem Commun 2004;10:16–17.
29. Mwenifumbo S, Shaffer MS, Stevens MM. Exploring cellular behaviour with multi-walled carbon nanotube constructs. J Mater Chem 2007;17:1894–1902.
30. Lu Q, Moore JM, Huang G, Mount AS, Rao AM, Larcom LL. RNA polymer translocation with single-walled carbon nanotubes. Nano Lett 2004;4:2473–2477.
31. Cherukuri P, Bachilo SM, Litovsky SH, Weisman RB. Near-infrared fluorescence microscopy of single-walled carbon nanotubes in phagocytic cells. J Am Chem Soc 2004;126:15638–15639.
32. Bianco A, Hoebeke J, Godefroy S, Chaioin O, Pantarotto D, Briand JP. Cationic carbon nanotubes bind to CpG oligodeoxynucleotides and enhance their immunostimulatory properties. J Am Chem Soc 2005;127:58–59.
33. Zanello LP, Zhao B, Hu H, Haddon RC. Bone cell proliferation on carbon nanotubes. Nano Lett 2006;6:562–567.
34. Hu H, Ni Y, Montana V, Haddon RC, Parpura V. Chemically functionalized carbon nanotubes as substrates for neuronal growth. Nano Lett 2004;4:507–511.
35. Chen X, Tam UC, Czlapinski JL, Lee GS, Rabuka D, Zettl A. Interfacing carbon nanotubes with living cells. J Am Chem Soc 2006;128:6292–6293.
36. Hu H, Ni Y, Mandal SK, Montana V, Zhao B, Haddon RC. Polyethyleneimine functionalized single-walled carbon nanotubes as a substrate for neuronal growth. J Phys Chem B 2005;109:4285–4289.
37. Kakudo N, Shimotsuma A, Miyake S, Kushida S, Kusumoto K. Bone tissue engineering using human adipose-derived stem cells and honeycomb collagen scaffold. J Biomed Mater Res A 2008;84:191–197.
38. Li HY, Zhai WY, Chang J. In vitro biocompatibility assessment of PHBV/Wollastonite composites. J Mater Sci Mater Med 2008;19:67–73.
39. Bai, H; Wang ZZ. Directing human embryonic stem cells to generate vascular progenitor cells. Gene Ther 2008;15:89–95.
40. Gosain AK, Riordan PA, Song LS, Amarante MT, Kalantarian B, Nagy PG, Wilson CR, Toth JM, McIntyre BL. A 1-year